Entrainment in laboratory analogs of cumulus and stratocumulus clouds tops

A. Gorska[1*,3], S. P. Malinowski[1,3], S. Blonski[2], J. Fugal[3,4], T. A. Kowalewski[2], P. Korczyk[2], W. Kumala[1]

[1] Institute of Geophysics, Faculty of Physics, University of Warsaw, Warsaw, Poland
[2] Institute of Fundamental Technological Research, Polish Academy of Sciences, Warsaw, Poland
[3] Institute of Atmospheric Physics, Johannes Gutenberg University, Mainz, Germany
[4] Max Planck Institute for Chemistry, Mainz, Germany

1. INTRODUCTION

Understanding entrainment of non–turbulent environmental air into turbulent convective clouds is still challenging (e.g. Wood, 2012; de Rooy et al., 2013). The aim of our experiment is to create laboratory analogs of cumulus and stratocumulus clouds tops in a cloud chamber. The goal is to study details of entraining structures by means of Particle Image Velocimetry (PIV).

There is a wide range of laboratory experiments which aim to investigate analogs of clouds and clouds processes. Entrainment into cumulus clouds has been first posted by Stommel (1947) and then studied in a series of laboratory experiments starting from e.g Scorer and Ronne (1956) and Woodward (1959). In case of stratocumulus cloud, theoretical work on entrainment started by Lilly (1968) was followed by laboratory experiments by Brown and Roshko (1974) and Broadwell and Breidenthal (1982). Nevertheless, details of entrainment into stratocumulus are poorly known and do not allow to formulate satisfactory parametrizations (Wood, 2012). Our experiment differs from many previous experiments due to the fact that the working media are real saturated air and water droplets. In our cloud chamber we observe two–phase evaporating flow, with realistic microphysics and effects of phase changes – evaporative cooling.

2. EXPERIMENTAL SETUP

For the purpose of the present study we modify an experimental setup used by Korczyk et al. (2012). Entrainment and mixing occur inside a cloud chamber (Fig. 1) of dimensions 1×1×1.8 m. The front wall of the chamber is transparent, while the others are covered by black foil to reduce laser light scattering. Cloud is produced by three ultrasonic humidifiers (Fig. 2), which outlets are directed into a container located under the chamber. A round opening in the floor of the chamber connects to the bottom container. On the top of the opening a stack (10 cm in diameter, 30 cm height) is placed, through which cloud comes out. Cloud droplets are lightened from the top of the chamber by a laser (Nd:YAG, wavelength: 532 nm, pulse energy: 0.9 mJ, pulse duration: 9 ns, pulse repetition rate: 1 kHz) light sheet (∼1 mm thick). Images of the light scattered by cloud droplets are recorded by a digital high speed CMOS camera (pco.imaging, resolution: 1280×1024 px, imaging frequency: 636 fps). Every 10 ms we record cross–sections images, collecting ∼700 frames

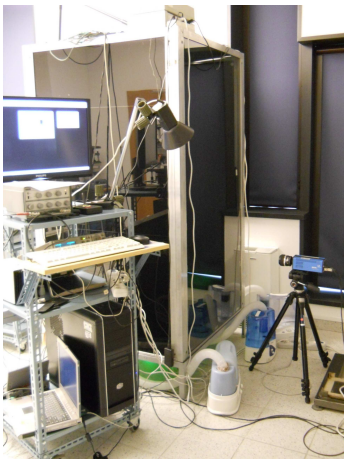

Figure 1: A view of the cloud chamber. One computer collects images recorded by the camera located in front of the glass wall of the chamber, two other computers collect temperature and humidity parameters. Three ultrasonic humidifiers produce cloud droplets.

*Corresponding author's address: Pasteura 7, 02–093 Warsaw; E-Mail: anna.gorska@igf.fuw.edu.pl

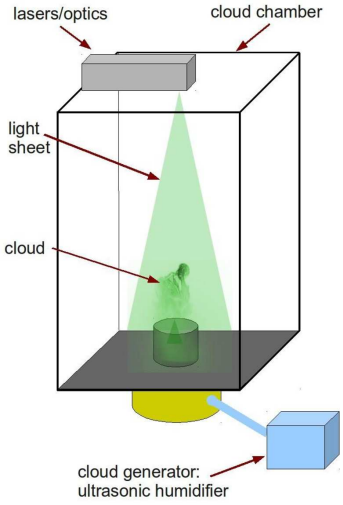

Figure 2: A scheme of the experimental setup. Cloud droplets scatter laser light sheet. They are generated by ultrasonic humidifier which outlet is directed into the container under the chamber. Cloud fills up the chamber through the stack.

in a series. Vertical profiles of temperature and humidity in the chamber are monitored by arrays of 15 thermocouples (located every 10 cm) and 4 capacitive sensors (located every 20 cm) placed close to the chamber wall.

3. DATA PROCESSING

Recording consecutive images, knowing time interval and using PIV technique enables to calculate two velocity components in the image plane. In order to retrieve velocities we use a newly developed algorithm based on a PIVKor algorithm (Korczyk et al., 2012). This is a multi–scale algorithm, identifying in a first step displacement of the largest structures in the flow and then, in a series of iterations, accounting for relative displacements of smaller and smaller patterns. Typical PIV algorithms, developed for more uniform distribution of flow markers than the distribution of droplets in the cloud chamber, fail to produce reliable velocity retrievals.

The original PIVKor algorithm is substantially modified in order to accelerate its execution. This allows to calculate velocities in long series of image pairs and study the evolution of entraining structures.

The modified algorithm was tested and calibrated on reference images (Okamoto et al., 2000). They are prepared in such a way, that diameters and locations of 4000 particles are randomly generated. Each particle brightness corresponds to the intensity of scattered light. Particles movement is calculated using predefined velocity data from numerical simulation (Fig. 3). The average velocity of simulated flow is 8.9 cm/s. Image size is 256×256 px, which corresponds to an area of 10×10 cm. Time interval between consecutive images is 33 ms. Laser light sheet thickness is 2 mm. In Fig. 3 simulated and retrieved velocity fields are compared, showing very good agreement in the velocity field pattern. Calculated mean relative error of velocity magnitude is ∼3.2 %.

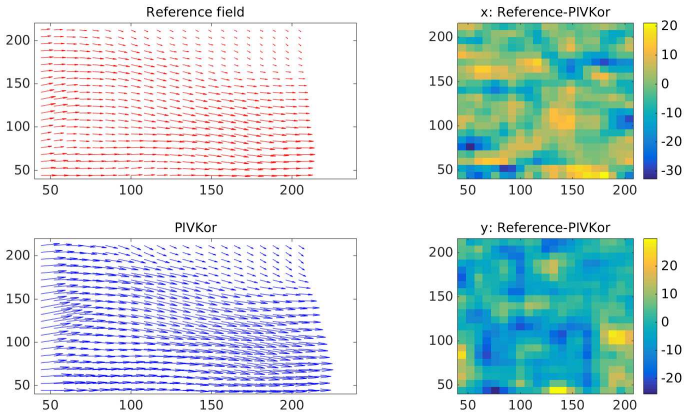

Figure 3: Modified PIVKor retrieved and reference velocity fields. Left panels show reference velocity field (upper) and velocity field obtained with PIVKor algorithm (lower). Right panels show differences between the components of velocity vectors (upper in horizontal direction and lower in vertical direction). Colorbar scale in (px/s). The mean relative error is ∼3.2 %.

4. INITIAL CONDITIONS

At the beginning of the experiment the air in the chamber is well mixed with the room air. Typical temperature (T_a) is ∼22 °C and relative humidity (RH_a) is ∼40 % (Fig. 4a). Then the cloudy plume, a negatively buoyant saturated air containing droplets of diameters ($\varnothing_d$) as observed in natural clouds (∼3–10 μm, Korczyk et al. (2012)), is gently pushed into the chamber through the stack (Fig. 4b). Liquid water content (LWC) in the plume is typically more than 10 g/kg – higher than in natural clouds (Korczyk et al., 2012, 2006). The plume temperature (T_c) is typically about 21 °C. The vertical velocity (w_c) at the stack top, measured by pressure velometer is ∼15 cm/s. The initial blob of cloudy air ascends up to 50 cm above the stack (h). Then negative buoyancy, enhanced by evaporative cooling in the course of mixing with the environment, causes blob collapse (Fig. 4c). The following portion of cloudy air leaving the stack interacts with the collapsing blob and spreads to the sides. Continuous gentle filling of the chamber through the stack leads to formation of a well mixed layer extending from the bottom of the chamber up to 50 cm above (H) (Fig. 4d). Mixing at the top of this layer with the unsaturated air from the upper part of the chamber and following evaporative cooling acts as cloud top entrainment instability and triggers downward convective motions which homogenize the cloudy layer. The temperature across the whole layer evolves, as illustrated in the consecutive temperature profiles in Fig. 4d. After few minutes stratification in the chamber corresponds to

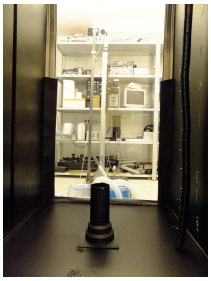

(a) initial conditions
$T_a \sim 22$ °C
$RH_a \sim 40$ %

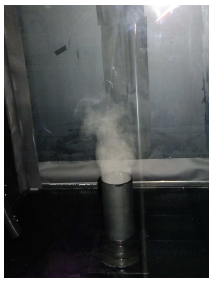

(b) initial blob
$\varnothing_d \sim 3 - 10$ μm
$LWC \sim 10$ g/kg
$T_c \sim 21$ °C
$w_c \sim 15$ cm/s
$h \sim 50$ cm

(c) evaporative cooling
negative buoyancy

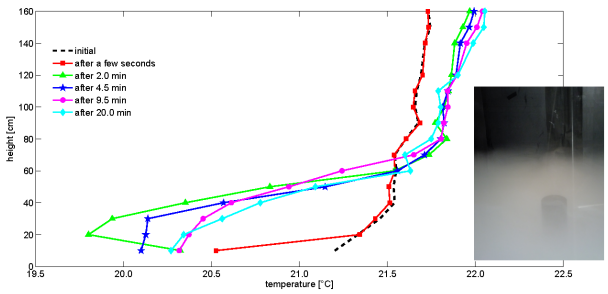

(d) temperature inversion
$H \sim 50$ cm
$\Delta T_{inv} \sim 2$ °C
$\Delta h_{inv} \sim 20$ cm

(e) ,,Cu”

(f) ,,Sc”

Figure 4: Initial conditions in the cloud chamber and the experiment evolution leading to formation of cumulus and stratocumulus clouds analogs. Used shortcuts: a–air, c–cloud, d–droplets, inv–inversion.

that observed often in the atmosphere: convective mixed boundary layer (here cloudy, resembling stratocumulus or fog), capped by a statically stable inversion and a weakly stable layer above. In the experimental conditions the temperature jump across the inversion (ΔT_{inv}) is about 2 °C and the depth of the inversion layer (Δh_{inv}) is ∼20 cm.

Having such a stable situation we are able to reproduce some aspects of two different types of convective clouds. We initiate either a strong updraft penetrating the inversion resembling an overshooting cumulus turret (Fig. 4e), or a weak updraft diverging below the inversion corresponding to a stratocumulus top (Fig. 4f).

5. OVERSHOOTING CUMULUS

First blob (Fig. 5a) of cloudy air moving through the stable layer of the cloud has large enough energy (vertical velocity ∼15 cm/s) to punch the inversion. Inversion penetration enhances divergence of the flow at the top of the starting plume. This results in the formation of a toroidal vortex ring (thermal) just above the stack outlet (Fig. 5b), capping the top of the updraft.

In the vertical cross–section the vortex ring can be seen as a two spirals on the both sides of the updraft. The spiral to the left of the turret circulates counterclockwise, while the right one rotates clockwise. The typical diameter of each ring is ∼4 cm. Clear air is entrained into the vortex interior from below, which is well documented by velocity vectors. Consecutive turnovers of the ring form a spiral structure of cloud–clear air filaments, nicely visible in the presented scenes.

The vortex ring forms a shell around the updraft core. Dilution of the vertical momentum due to entrainment of still environmental air into the vortex ring and increasing negative buoyancy due to interfacial mixing at the borders between cloudy and clear air filaments decelerate the shell. Meanwhile, the undiluted updraft core ascends with almost constant velocity. This results in vertical elongation of the shell (Fig. 5c). The flow becomes less organized and instabilities and secondary eddies appear. The shell (originally the vortex ring) begins to collapse, the unprotected updraft core quickly mixes with the environment and also goes down (Fig. 5d). Collapsing cloud volumes collide with the lower portions of the updraft and the cloud diverges, mixing into the ,,boundary layer”.

Vortex rings are expected features on top of cumulus clouds. The overall behaviour of the laboratory analog of overshooting cumulus top is in agreement with many earlier studies and observations. Damiani et al. (2006) presents several examples of velocity retrievals in the top of active cumulus turret obtained with use of airborne dual–Doppler radar. Evolution of the vortex ring reported in Damiani and Vali (2007) especially its ascent in the course of cloud development, corresponds well to our experiments, despite different dynamics of the updraft core (positive buoyancy in natural clouds, forced ascent of a negatively buoyant plume in our case). There are,

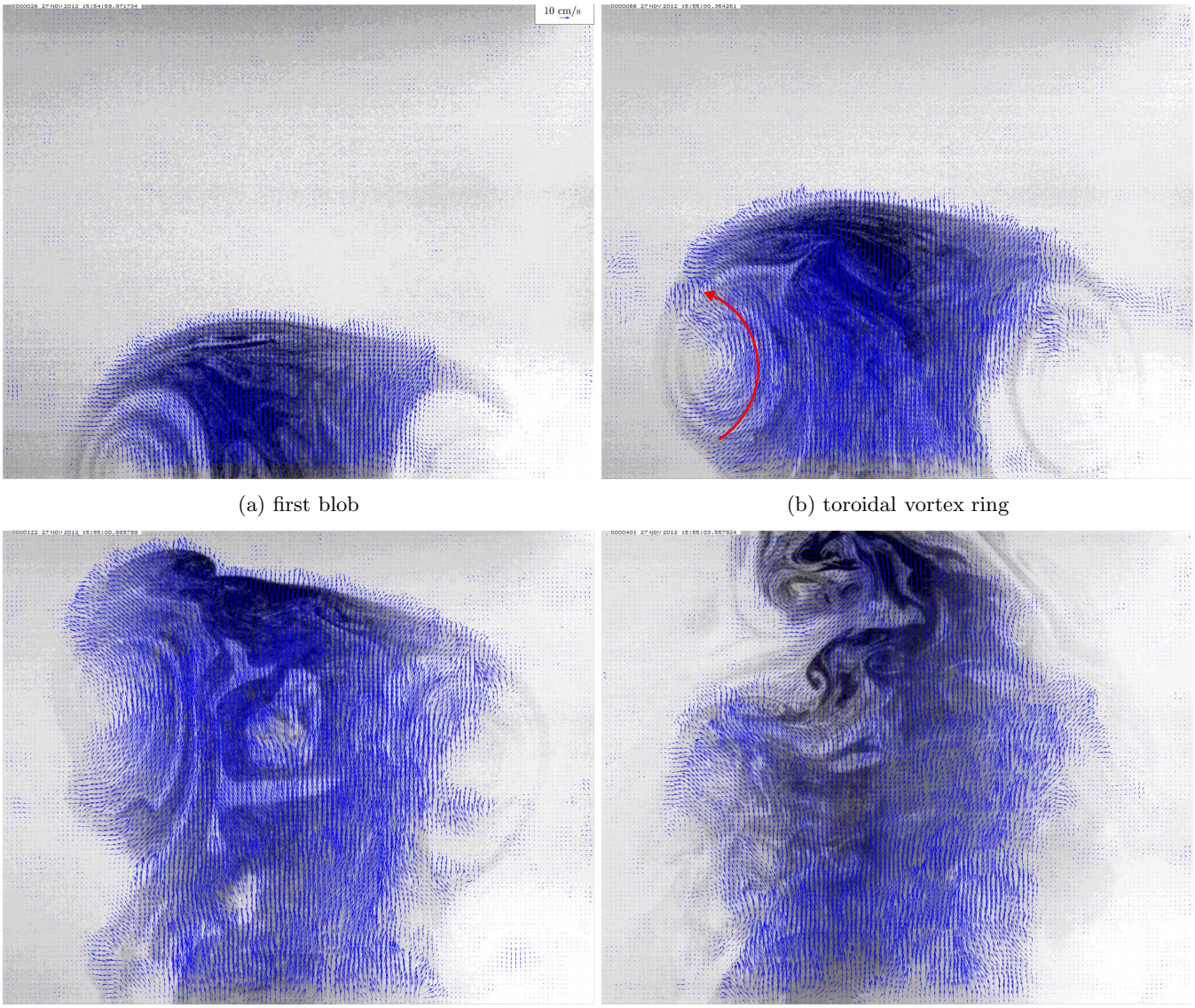

(a) first blob

(b) toroidal vortex ring

(c) shell vertical elongation

(d) cloud collapse

Figure 5: A vertical cross–sections through the evolution of the vortex ring at the top of an updraft penetrating the inversion layer (negative images). An area corresponds to about 13×10 cm. Rotation of the toroid causes that entrained still air from below the ring forms cloud–clear air filaments.

also, many differences. First, vortex structures in natural clouds are less regular than in our laboratory analog. Second, the geometry of these structures seems different: the ratio of the diameter of the torus to the diameter of the vortex ring is larger in nature than in the laboratory experiment. While the first effect can be attributed to a much greater range of scales in natural clouds than we are able to model in the cloud chamber, the second one can be tested in the future with a stack of a larger diameter.

6. STRATOCUMULUS TOP

When cloudy air leaving the stack is slower (vertical velocity ∼10 cm/s), its kinetic energy does not allow to punch through the inversion. In such a situation the flow impinges upon the inversion, lifts the inversion layer up by a few cm and diverges to the sides. The maximum horizontal velocity of the diverging flow is located just below the inversion top. The horizontal outflow produces a shear layer at the cloud top. This triggers Kelvin–Helmholtz instabilities and produces small (typical diameter of ∼2 cm) vortices of a rotation opposite to that observed in the vortex rings of overshooting cumulus (Fig. 6).

Initial stages of such vortices can be recognized in the velocity patterns at the cloud top. Portions of dry air from above the inversion are captured by circulation, which can be noticed on the shades of grey in the image. The following interfacial mixing inside small vortices and resulting evaporative cooling form intrusions, which sink into the well mixed layer below captured into vortices.

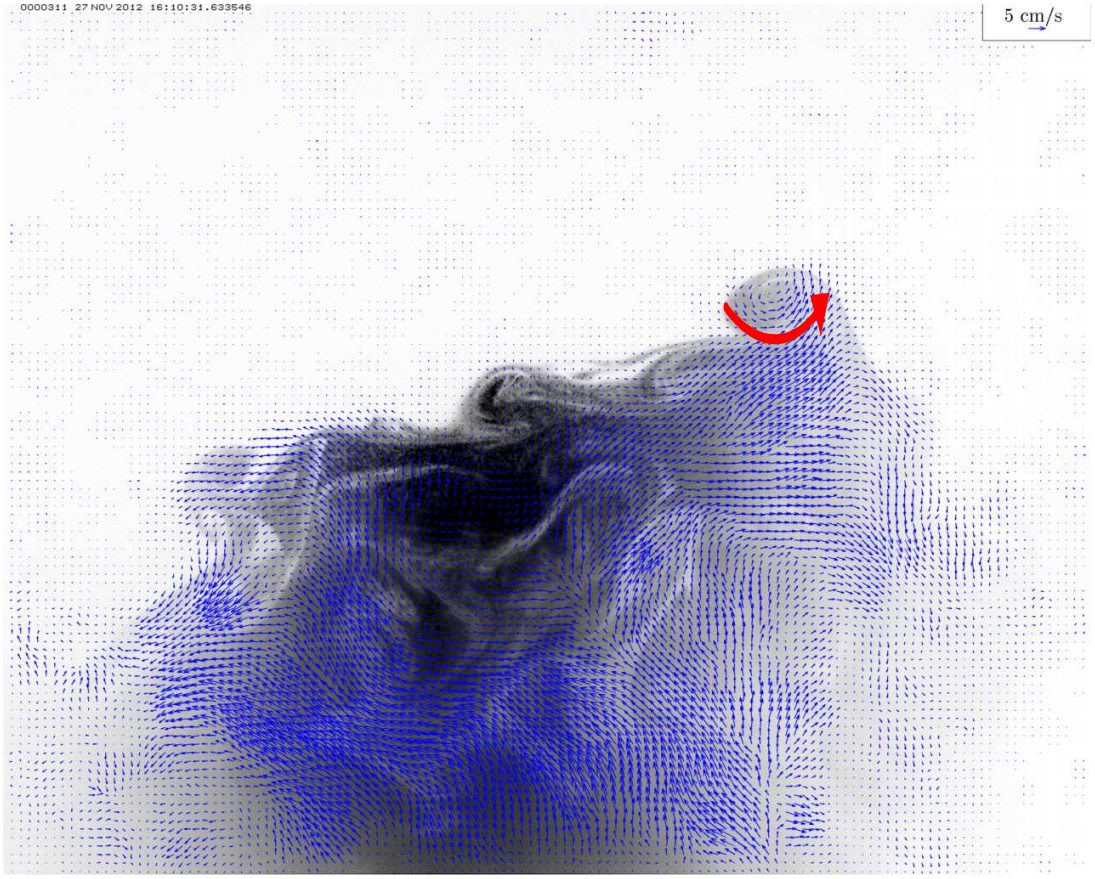

(a)

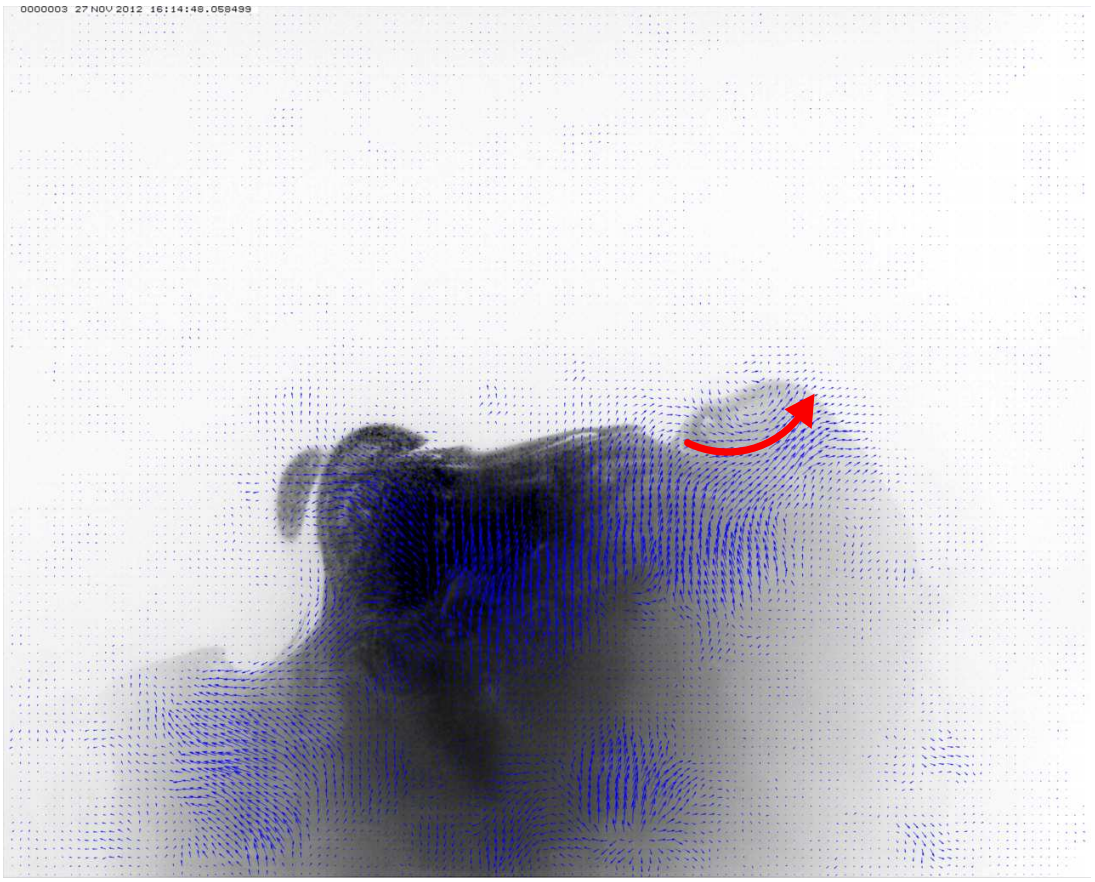

(b)

Figure 6: A cross–sections through an updraft impinging upon inversion (negative images). An area corresponds to about 13×10 cm. Portions of dry air from above the inversion are captured by circulation and form intrusions, which entrain still air into the well mixed layer below.

Stratocumulus top observed in the chamber resembles results of Large Eddy Simulations by Kurowski et al. (2009). The authors report the presence of updrafts impinging upon inversion, divergence of the updrafts at the cloud top, development of turbulence and the overall flow pattern similar to what we observe in the cloud chamber. The resolution of simulations does not allow to look into details of entraining structures, in the course of later experiments we will focus on analysis of these small–scale details. Another evidence of similarities of our results with in–situ observations can be find in Katzwinkel et al. (2012) and Malinowski et al. (2013). They show that in the case of horizontal wind shear across the cloud top and capping inversion the gradient Richardson number allows for dynamical instability and formation of entraining eddies. The difference is that in these studies the shear is not resulting from divergence of the updraft.

7. CONCLUSIONS

Preliminary results of our new laboratory setup aimed at investigation of entrainment into surrogates of convective clouds, demonstrated that reproduction of some features of cloud topped boundary layer in the laboratory cloud chamber is possible. In particular, we are able to reproduce static stability profile across the boundary layer, temperature inversion and free troposphere and to simulate in such conditions two different cases: an analog of overshooting cumulus and an analog of updraft in stratocumulus. Visualization of these cases with a laser light sheet technique and adoption of the PIV allows to compare the observed entrainment/mixing patterns with observations in natural clouds and numerical simulations.

We have shown that entraining eddies in stratocumulus and cumulus cases rotate in different directions. In the future we plan to expand the experiment to account for various flow configurations and perform more quantitative studies of entrainment.

ACKNOWLEDGEMENTS
This research was supported by the Polish National Science Centre with the grant 2013/08/A/ST10/00291.

References

Broadwell, J. E., and R. E. Breidenthal, 1982: Simple model of mixing and chemical reaction in a turbulent shear layer. *J. Fluid Mech.*, **125**, 397–410.

Brown, G. L., and A. Roshko, 1974: On density effects and large structure in turbulent mixing layer. *J. Fluid Mech.*, **64**, 775–816.

Damiani, R., and G. Vali, 2007: Evidence for tilted toroidal circulations in cumulus. *J. Atmos. Sci.*, **64 (6)**, 2045–2060.

Damiani, R., G. Vali, and S. Haimov, 2006: The Structure of Thermals in Cumulus from Airborne Dual–Doppler Radar Observations. *J. Atmos. Sci.*, **63**, 1432–1450.

de Rooy, W. C., and Coauthors, 2013: Entrainment and detrainment in cumulus convection: an overview. *Q. J. R. Meteorol. Soc.*, **139**, 1–19.

Katzwinkel, J., H. Siebert, and R. A. Shaw, 2012: Observation of a Self–Limiting, Shear–Induced Turbulent Inversion Layer Above Marine Stratocumulus. *Boundary-Layer Meteorol.*, **145**, 131–143.

Korczyk, P., S. P. Malinowski, and T. A. Kowalewski, 2006: Mixing of cloud and clear air in centimeter scales observed in laboratory by means of Particle Image Velocimetry. *Atmos. Res.*, **82**, 173–182.

Korczyk, P. M., T. A. Kowalewski, and S. P. Malinowski, 2012: Turbulent mixing of clouds with the environment: Small scale two phase evaporating flow investigated in a laboratory by particle image velocimetry. *PhysicaD*, **241**, 288–296.

Kurowski, M. J., S. P. Malinowski, and W. W. Grabowski, 2009: A numerical investigation of entrainment and transport within a strotocumulus–topped boundary layer. *Q. J. R. Meteorol. Soc.*, **135 (638)**, 77–92.

Lilly, D. K., 1968: Models of cloud-topped mixed layers under a strong inversion. *Q. J. Roy. Meteor. Soc.*, **94**, 292–309, doi:10.1002/qj.49709440106.

Malinowski, S. P., H. Gerber, I. Jen-LaPlante, M. K. Kopeć, W. Kumala, K. Nurowska, P. Y. Chuang, and K. E. Haman, 2013: Physics of stratocumulus top (POST): turbulent mixing across capping inversion. *Submitted to Atmos. Chem. Phys.*

Okamoto, K., S. Nishio, T. Saga, and T. Kobayashi, 2000: Standard images for particle-image velocimetry. *Meas. Sci. Technol.*, **11**, 685–691.

Scorer, R. S., and C. Ronne, 1956: Experiments with convection bubbles. *Weather*, **11**, 151–155.

Stommel, H., 1947: Entrainment of air into a cumulus cloud. *J. Meteor.*, **4**, 91–94.

Wood, R., 2012: Stratocumulus Clouds. *Mon. Wea. Rev.*, **140 (8)**, 2373–2423.

Woodward, B., 1959: The motion in and around isolated thermals. *Quarl. J. Roy. Meteor. Soc.*, **85**, 144–151.